

Comparative study between sliding mode and Neuro-fuzzy controllers for a water pump drive supplied by multi-level converters

The primary objective of this paper is to investigate nonlinear control techniques for regulating the speed and phase currents of a dual-star induction motor (DSIM) driving a water pump. This pumping system is powered by multilevel converters (MLC). The control of this system is based on a sliding mode controller (SMC) and a Neuro-fuzzy logic controller (NFLC). Additionally, this system is implemented with indirect field-oriented control (IFOC). To control this system, two voltage-source multilevel converters (VSMC) employing pulse width modulation (PWM) methods are applied. Accordingly, a four-layer artificial neural network (ANN) structure is utilized to train the parameters of the fuzzy logic controller (FLC) by minimizing the square of the error. The obtained simulation and experimental results are highly satisfactory and demonstrate that the performance of the NFLC is enhanced by employing two MLC, introducing load disturbances and parameter variations compared to other techniques.

Keywords: Dual star induction machine, sliding mode controller; indirect field oriented control, multi-level converters, Neuro fuzzy logic controller.

1. Introduction

The DSIM driving a water pump powered by a voltage source MLC presents several advantages over traditional three-phase induction motors driving a water pump (Fig.1). These benefits encompass reduced harmonic currents within the rotor and diminished current per phase, all without necessitating an increase in voltage per phase compared with three-phase induction machine [1-4]. This leads to enhanced reliability and minimized torque pulsations, as illustrated in Fig 1 [4-3]. The DSIM is structured with two windings spatially offset by $\alpha = 30^\circ$ electrical degrees, each possessing isolated neutrals, as depicted in Figure 1 [4-5]. The interaction between the field and torque is addressed. To tackle this challenge, vector control techniques have been devised, allowing for decoupling between the field and torque, akin to control principles applied in DC machines [7]. Particularly, the indirect vector control approach for the dual stator winding induction machine assumes that the machine functions as two independent induction machines interconnected through the same rotor shaft [8-9]. This method has demonstrated effectiveness in attaining precise control over these robust machines, thereby broadening their adaptability across various industrial domains.

* Corresponding author: E. Zaidi, Department of Irrigation and Drainage, National Higher School for Hydraulics, 29 route de Soumaa, Blida, Algeria, E-mail: e.zaidi@ensh.dz

¹Department of Irrigation and Drainage, National Higher School for Hydraulics, 29 route de Soumaa, Blida, Algeria

²Faculty of Sciences and Technology, University Mohamed El Bachir El Ibrahimi of Bordj Bou Arreridj, Algeria.

The conventional control algorithms, like **PI** and **PID** controllers, exhibit notable limitations necessitating enhancement, its performance cannot be optimized in the event of a failure[1-2].They are susceptible to fluctuations in system parameters, encounter challenges in managing internal disturbances and load variations, and depend heavily on precise machine models with predefined parameters [8-10]. Limited ability to deal with nonlinearities, which degrades performance under variable conditions, may lead to steady-state errors. The tuning process can be complex to achieve optimal performance [8-11]. Conversely, intelligent controller designs offer a promising alternative by not mandating the exact mathematical model of drive systems. Consequently, there arises a burgeoning demand to prioritize intelligent controllers when aiming to regulate the speed of high-performance induction machine drive systems [5-8].

Several novel control methods have been proposed as alternatives to traditional **PI** and **PID** techniques. These include fuzzy logic controller (**FLC**) and artificial neural networks (**ANNs**). However, while **FLC** offer a simple solution for machine drive speed control, their effectiveness is limited to a narrow operating range. Achieving optimal performance often requires extensive manual fine-tuning through trial and error [12]. Conversely, training **ANNs** to handle all possible operating modes necessitates a comprehensive dataset, which can be a significant challenge [9]. Targeting the specific control needs of induction machine drives, researchers have developed the Neuro-Fuzzy Logic Controller (**NFLC**) [13-15]. This innovative controller leverages the complementary strengths of **FLC** and artificial neural networks (**ANNs**).The **FLC** excel at incorporating human expertise through interpretable rules, while **ANNs** demonstrate exceptional capabilities in learning complex, non-linear relationships. By combining these functionalities, the **NFLC** aims to achieve superior performance and efficiency in terms of speed regulation and energy consumption compared to traditional control methods.

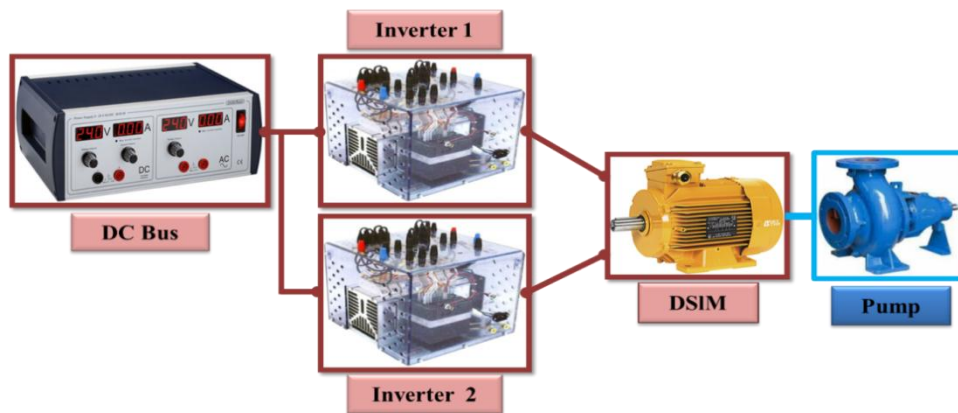


Fig. 1. Design of a pumping system based on the DSIN Fed by two MLC.

The developed simulation model employs **IFOC** for a **DSIM** driving a water pump powered by two **MLC**. This model fully integrates the proposed **NFLC** and **SMC** controllers. Simulation and experimental results effectively demonstrate that the **NFLC** exhibits superior performance under real-world scenarios, suggesting its potential to significantly advance the field of intelligent control systems for pumping system drives

2. DSIM driving a water pump modeling

The DSIM driving a water pump is configured with two groups of three-phase windings, each spatially shifted by 30 electrical degrees [5-10], and they share a single stator magnetic core, as depicted in Fig. 2[16]. However, dealing with modeling and controlling the DSIM in its native reference frame poses considerable hurdles. To address these obstacles, acquiring a streamlined model becomes essential. As a result, the mathematical modeling technique for the DSIM closely mirrors that of conventional induction machines, frequently utilizing analogous simplification assumptions [5-17-18]:

- ❖ *Motor windings undergo sinusoidal distribution;*
- ❖ *Both sets of windings have identical parameters;*
- ❖ *The flux path within the motor is linear;*
- ❖ *The model incorporates mutual leakage inductances.*

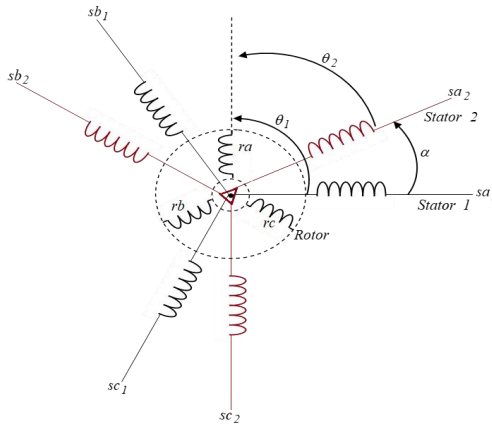


Fig. 1. Windings of the dual stator induction motor.

We can express the equation for the stator voltages as:

$$\begin{cases} v_{ds1} = R_s i_{ds1} + \frac{d\lambda_{ds1}}{dt} - \omega_s \lambda_{qs1} \\ v_{qs1} = R_s i_{qs1} + \frac{d\lambda_{qs1}}{dt} + \omega_s \lambda_{ds1} \end{cases} \quad (1)$$

$$\begin{cases} v_{ds2} = R_s i_{ds2} + \frac{d\lambda_{ds2}}{dt} - \omega_s \lambda_{qs2} \\ v_{qs2} = R_s i_{qs2} + \frac{d\lambda_{qs2}}{dt} + \omega_s \lambda_{ds2} \end{cases} \quad (2)$$

The equation for the rotor voltages is given by:

$$\begin{cases} 0 = R_r i_{dr} + \frac{d\lambda_{dr}}{dt} - (\omega_s - \omega_r) \lambda_{qr} \\ 0 = R_r i_{qr} + \frac{d\lambda_{qr}}{dt} + (\omega_s - \omega_r) \lambda_{dr} \end{cases} \quad (3)$$

The equation for the rotor and the stator flux linkages are:

$$\begin{cases} \lambda_{ds1} = l_s i_{ds1} + L_m(i_{ds1} + i_{ds2} + i_{dr}) \\ \lambda_{qs1} = l_s i_{qs1} + L_m(i_{qs1} + i_{qs2} + i_{qr}) \end{cases} \quad (4)$$

$$\begin{cases} \lambda_{ds2} = l_s i_{ds2} + L_m(i_{ds1} + i_{ds2} + i_{dr}) \\ \lambda_{qs2} = l_s i_{qs2} + L_m(i_{qs1} + i_{qs2} + i_{qr}) \end{cases} \quad (5)$$

$$\begin{cases} \lambda_{dr} = l_r i_{dr} + L_m(i_{ds1} + i_{ds2} + i_{dr}) \\ \lambda_{qr} = l_r i_{qr} + L_m(i_{qs1} + i_{qs2} + i_{qr}) \end{cases} \quad (6)$$

2.1. Mechanical Equation

The rotor speed can be expressed as:

$$J \frac{d\omega_r}{dt} = C_{em} - C_r - f \omega_r \quad (7)$$

The electromagnetic torque of the **DSIM** is given as:

$$C_{em} = P \frac{L_m}{L_m + L_r} (\lambda_{dr}(i_{qs1} + i_{qs2}) - \lambda_{qr}(i_{qs1} + i_{qs2})) \quad (8)$$

Where: ω_s, ω_r : the speed of the synchronous reference frame and the electrical angular velocity of the rotor; L_{s12} and L_r inductances of stator and rotor ; J : moment of inertia L_m : resultant magnetizing inductance; P : number of pole pairs; λ : flux; C_r : load torque; f : total viscous friction coefficient.

The **IFOC** serves as the main objective to enable autonomous manipulation of the rotor flux and electromagnetic torque of a machine, akin to the approach employed in **DC** machines [9,13,17]. So, utilizing the **IFOC** method in the **DSIM** driving a water pump simplifies the control strategy and enhances the model is designed in [10-12].

3. Multi-level Converters Model

The cascade H-bridge multi-level converters (**CHMLC**) offer numerous advantages over conventional bipolar inverters, particularly in industrial drive systems. These advantages include improved electromagnetic compatibility, reduced voltage stress on switches, and decreased harmonic content at higher levels, resulting in decreased reliance on filters and a more refined output voltage waveform with minimal Total Harmonic Distortion (**THD**) [5,12]. Among the various topologies of multi-level converters, the diode-clamped, flying capacitor, and cascade H-bridge structures (Fig. 4) emerge as the most favored choices [19]. These advancements in converter technology bring significant enhancements in efficiency and performance for industrial drive applications.

For instance, the proposed multi-level three-phase cascaded H-bridge converters, such as the seven-level topology, consist of standard three-leg converters (one leg for each phase) with an H-bridge in series with each converter leg, as depicted in Fig. 4 [17-18]. All signals for controlling the **CHMLC** are generated using a **PWM** signal modulation technique. The most popular and easiest technique for controlling the active devices involves several triangle carrier signals and one reference signal, as illustrated in Fig. 3.

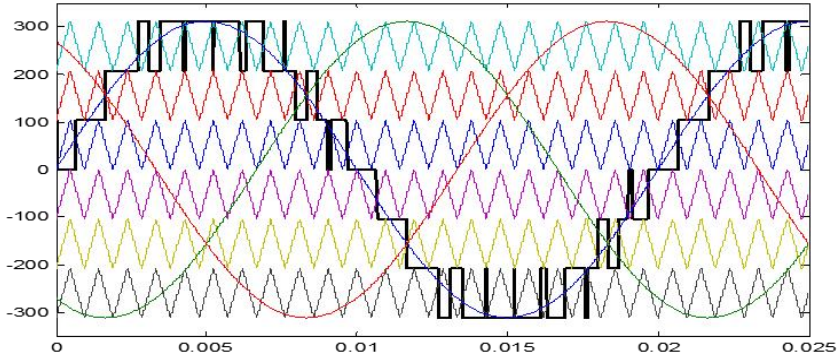


Fig. 3. A principle of multi-carrier PWM strategy for MLC with seven levels.

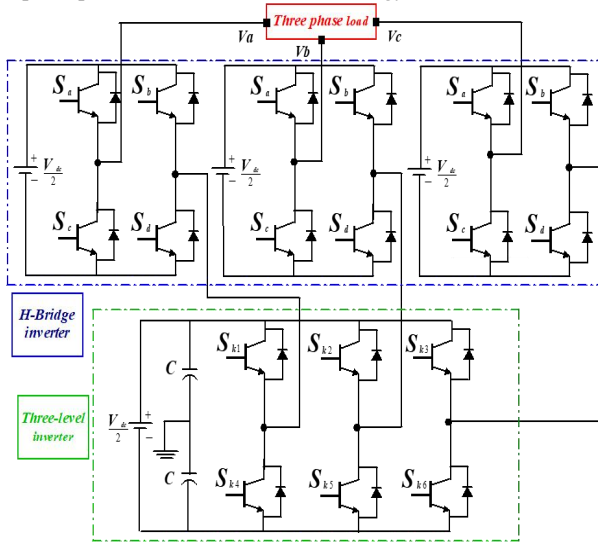


Fig. 4. The topology of the seven level three-phase CHMLC.

4. DSIM driving a water pumping SMC method

The operating principle of sliding mode control is based on defining a sliding surface, which represents the difference between the desired state of the system and its actual state [12,16]. The control is designed to drive the systems state to converge to the sliding surface within a finite time. Once the system reaches the sliding surface, it remains constrained to this surface, even in the presence of disturbances [12,16].

4.1. Speed control using SMC

The sliding surface for speed control with relative degree $r=1$ is given by the following formula:

$$S(\Omega) = \Omega_{Ref} - \Omega_m \tag{9}$$

The derivative of the sliding surface is:

$$\dot{S}(\Omega) = \dot{\Omega}_{Ref} - \dot{\Omega}_m \tag{11}$$

For the speed to converge to its desired reference value, two conditions must be satisfied: the first condition is that the sliding surface and its derivative are zero, and the second condition is that the Lyapunov attractively relation is less than

zero(Fig. 5). By revisiting the equation of mechanical speed and substituting the derivatives of the speed and its reference $\dot{\Omega}_m$ and Ω_{Ref} , we obtain the following relation:

$$\dot{S}(\Omega) = \dot{\Omega}_{Ref} - \frac{1}{J}C_{em} + \frac{1}{J}C_r + \frac{f}{J}\Omega_m \tag{12}$$

where:

$$I_{sq} = I_{sq_eq} + I_{sq_dis} \tag{13}$$

By substituting expression (13) into expression (12), the control appears in the following equation:

$$\dot{S}(\Omega) = \dot{\Omega}_{Ref} - \frac{K_{wr}\phi_r}{J}(I_{sq_eq} + I_{sq_dis}) + \frac{1}{J}C_r + \frac{f}{J}\Omega_m \tag{14}$$

with:

$$K_{wr} = \frac{p.M}{L_r}$$

Under the application of sliding mode control (SMC) in steady state, the following conditions are met: $S(\Omega) = 0, \dot{S}(\Omega) = 0$ and $I_{sq_dis} = 0$. Consequently, the equivalent control law is expressed as follows:

$$I_{sq_eq} = \frac{J}{K_{wr}\phi_r}\dot{\Omega}_{Ref} + \frac{1}{K_{wr}\phi_r}C_r + \frac{f}{K_{wr}\phi_r}\Omega_m \tag{15}$$

Also, the discontinuous control is given by the following formula:

$$I_{sq_dis} = K_{sq} \cdot \text{sat}S(\Omega) \tag{16}$$

To verify the stability condition of the system, the parameter K_{sq} must be a positive gain. Finally, the speed control law by SMC is synthesized as follows:

$$I_{sq} = \frac{J}{K_{wr}\phi_r}\dot{\Omega}_{Ref} + \frac{1}{K_{wr}\phi_r}C_r + \frac{f}{K_{wr}\phi_r}\Omega_m + K_{sq} \cdot \text{sat}S(\Omega) \tag{17}$$

4.2. Control of phase currents by SMC

In the control of stator currents of the DSIM driving a water pump powered by two parallel inverters, the sliding surfaces are defined as follows:

$$\begin{cases} S(I_{sd1}) = I_{sd1_Ref} - I_{sd1} \\ S(I_{sd2}) = I_{sd2_Ref} - I_{sd2} \\ S(I_{sq1}) = I_{sq1_Ref} - I_{sq1} \\ S(I_{sq2}) = I_{sq2_Ref} - I_{sq2} \end{cases} \tag{18}$$

The derivatives of the sliding surfaces are:

$$\begin{cases} \dot{S}(I_{sd1}) = \dot{I}_{sd1_Ref} - \dot{I}_{sd1} \\ \dot{S}(I_{sd2}) = \dot{I}_{sd2_Ref} - \dot{I}_{sd2} \\ \dot{S}(I_{sq1}) = \dot{I}_{sq1_Ref} - \dot{I}_{sq1} \\ \dot{S}(I_{sq2}) = \dot{I}_{sq2_Ref} - \dot{I}_{sq2} \end{cases} \tag{19}$$

Once the sliding surface is defined, the next step is to determine the equivalent control and the discontinuous control so that the variable to be regulated converges towards the sliding surface, and then towards its equilibrium point. Consequently, the necessary condition for calculating the equivalent controls is represented by the following equations:

$$\begin{cases} S(I_{sd1}) = 0 \\ S(I_{sd2}) = 0 \\ S(I_{sq1}) = 0 \\ S(I_{sq2}) = 0 \end{cases} \quad \text{and} \quad \begin{cases} \dot{S}(I_{sd1}) = 0 \\ \dot{S}(I_{sd2}) = 0 \\ \dot{S}(I_{sq1}) = 0 \\ \dot{S}(I_{sq2}) = 0 \end{cases} \quad (20)$$

Replacing the derivatives of currents and references from equations (20) into the equations (1) and (2), we obtain the following expressions:

$$\begin{cases} \dot{S}(I_{sd1}) = \dot{I}_{sd1_Ref} - a_1 V_{sd1} + a_2 I_{sd1} + a_3 \dot{\phi}_r - \omega_s I_{sq1} \\ \dot{S}(I_{sd2}) = \dot{I}_{sd2_Ref} - a_1 V_{sd2} + a_2 I_{sd2} + a_3 \dot{\phi}_r - \omega_s I_{sq2} \\ \dot{S}(I_{sq1}) = \dot{I}_{sq1_Ref} - a_1 V_{sq1} + a_2 I_{sq1} + a_3 \omega_s \phi_r + \omega_s I_{sd1} \\ \dot{S}(I_{sq2}) = \dot{I}_{sq2_Ref} - a_1 V_{sq2} + a_2 I_{sq2} + a_3 \omega_s \phi_r + \omega_s I_{sd2} \end{cases} \quad (21)$$

with:

$$\begin{cases} a_1 = \frac{1}{\sigma L_s} \\ a_2 = \frac{R_s}{\sigma L_s} \\ a_3 = \frac{M}{\sigma L_s L_r} \end{cases}$$

where :

$$\begin{cases} V_{sd1} = V_{sd1_eq} + V_{sd1_dis} \\ V_{sd2} = V_{sd2_eq} + V_{sd2_dis} \\ V_{sq1} = V_{sq1_eq} + V_{sq1_dis} \\ V_{sq2} = V_{sq2_eq} + V_{sq2_dis} \end{cases} \quad (22)$$

The development of the calculation of equivalent controls is given by the following expressions:

$$\begin{cases} V_{sd1_eq} = \frac{1}{a_1} \dot{I}_{sd1_Ref} + \frac{a_2}{a_1} I_{sd1} + \frac{a_3}{a_1} \dot{\phi}_r - \frac{1}{a_1} \omega_s I_{sq1} \\ V_{sd2_eq} = \frac{1}{a_1} \dot{I}_{sd2_Ref} + \frac{a_2}{a_1} I_{sd2} + \frac{a_3}{a_1} \dot{\phi}_r - \frac{1}{a_1} \omega_s I_{sq2} \\ V_{sq1_eq} = \frac{1}{a_1} \dot{I}_{sq1_Ref} + \frac{a_2}{a_1} I_{sq1} + \frac{a_3}{a_1} \omega_s \phi_r + \frac{1}{a_1} \omega_s I_{sd1} \\ V_{sq2_eq} = \frac{1}{a_1} \dot{I}_{sq2_Ref} + \frac{a_2}{a_1} I_{sq2} + \frac{a_3}{a_1} \omega_s \phi_r + \frac{1}{a_1} \omega_s I_{sd2} \end{cases} \quad (23)$$

Therefore, the discontinuous controls are given by the following formulas:

$$\begin{cases} V_{sd1_dis} = K_{sd1} \cdot \text{satS}(I_{sd1}) \\ V_{sd2_dis} = K_{sd2} \cdot \text{satS}(I_{sd2}) \\ V_{sq1_dis} = K_{sq1} \cdot \text{satS}(I_{sq1}) \\ V_{sq2_dis} = K_{sq2} \cdot \text{satS}(I_{sq2}) \end{cases} \quad (24)$$

where : K_{sd1} , K_{sd2} , K_{sq1} et K_{sq2} are positive gains.

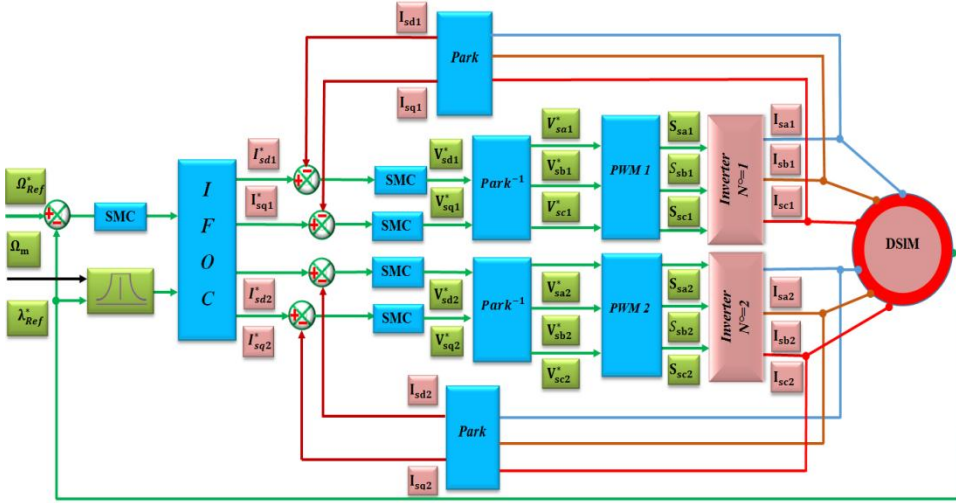


Fig. 5. Block diagram of a DSIN based pumping system powered by two MLC using an SMC controller.

5. DSIMUsing Neuro-Fuzzy Controller methode

The **NFLC** system integrates an online learning algorithm with a Neuro-fuzzy network, depicted visually in Fig. 2. The Neuro-fuzzy network undergoes intensive training utilizing the online learning algorithm. To facilitate the fuzzy inference process, the system features two inputs: 'speed error' and its rate of change, denoted as 'input 1' and 'input 2', respectively [12]. The desired output, referred to as the 'torque command,' is generated as the system's output [14]. The architecture of the artificial neural network (ANN) is depicted in Fig. 5, comprising four distinct layers. The first layer manages inputs, the second layer handles Fuzzification, the third layer performs vital fuzzy rule evaluation, and the fourth layer oversees the Defuzzification process [1217].

The desired electromagnetic torque C_{em}^* is achieved through the implementation of a **SMC** controller. In this context, the term 'error' refers to the disparity between the desired torque C_{em}^* and the control torque C_{em-NFC} , which is currently being generated by the neuro-fuzzy controller.

5.1. Back propagation algorithm

Detailed discussions on the various layers of the Neuro-Fuzzy network are provided below:

First layer:Each input node within this layer corresponds to a specific input variable. The inputs to this layer are provided by the variables: 'speed error' and its rate of change, identified as 'input 1' and 'input 2,' respectively.

$$net_1^I = e_\omega \text{ and } net_2^I = e_\omega^* .$$

The outputs of this layer are given by:

$$y_1^I = f_1^I(net_1^I) = e_\omega \text{ and } y_2^I = f_2^I(net_2^I) = e_\omega^* .$$

The weights of this layer are unity and fixed.

Second layer:Each node executes a membership function, which can be termed as the Fuzzification process. Specifically, each input is associated with seven Gaussian membership functions (MFs), as illustrated in Fig. 6.

$$net_{1,j}^{II} = - \left(\frac{x_{1,j}^{II} - m_{1,j}^{II}}{\sigma_{1,j}^{II}} \right)^2 \tag{25}$$

$$net_{2,k}^{II} = - \left(\frac{x_{2,k}^{II} - m_{2,k}^{II}}{\sigma_{2,k}^{II}} \right)^2 \tag{26}$$

$$\begin{cases} y_{1,j}^{II} = f_{1,j}^{II}(net_{1,j}^{II}) = e^{net_{1,j}^{II}} \\ y_{2,k}^{II} = f_{2,k}^{II}(net_{2,k}^{II}) = e^{net_{2,k}^{II}} \end{cases} \tag{27}$$

where $m_{1,j}^{II}, m_{2,k}^{II}$: represents the Gaussian MFs centers and $\sigma_{1,j}^{II}, \sigma_{2,k}^{II}$: determines the MFs widths.

Third layer:This layer is referred to as the inference and decision layer. The output of each node is determined by the product of all input signals. With a rule base comprising 49 rules in the fuzzy inference system, the rule base of the Neuro-Fuzzy controller is outlined in Table 1. In this layer, there are 49 nodes, each serving the function of performing inference and decision-making based on the inputs and the rules defined in the rule base:

Table. 1. Rules base for FLC controller.

e \ de	NB	NM	NS	ZE	PS	PM	PB
PB	ZE	NS	NM	NB	NB	NB	NB
PM	PS	ZE	NS	NM	NB	NB	NB
PS	PM	PS	ZE	NS	NM	NB	NB
ZE	PB	PM	PS	ZE	NS	NM	NB
NS	PB	PB	PM	PS	ZE	NS	NM
NM	PB	PB	PB	PM	PS	ZE	NS
NB	PB	PB	PB	PB	PM	PS	ZE

The values of weights between second layer and third layer are unity.

Fourth layer: This layer is known as the Defuzzifier layer, and it utilizes the center of gravity method to determine the output of the NFLC. The equation for each node is specified as follows:

$$a = \sum_j \sum_k (\omega_{jk}^{IV} y_{jk}^{III}), b = \sum_j \sum_k (y_{jk}^{III}) \tag{26}$$

$$\text{net}_0^{IV} = \frac{a}{b}, y_0^{IV} = f_0^V = \frac{a}{b} \tag{27}$$

ω_{jk}^{IV} : specify the values of the output membership functions used in the FLC, $\omega_0^{IV} y_0^{IV}$ is an output of the defuzzification layer a and b are the numerator and the denominator of the function used in the center of area technique, respectively. In the NFLC, the object of the learning algorithm is correction the weights ω_{jk}^{IV} , the $m_{1,j}^{II}, m_{2,k}^{II}$ and $\sigma_{1,j}^{II}, \sigma_{2,k}^{II}$. For the learning algorithm, we use the supervised gradient descent method. Therefore, the error E we take for describe the back propagation algorithm.

$$E(l) = \frac{1}{2} e_{c_{em}}^2 \tag{28}$$

$$e_{c_{em}} = d - y \tag{29}$$

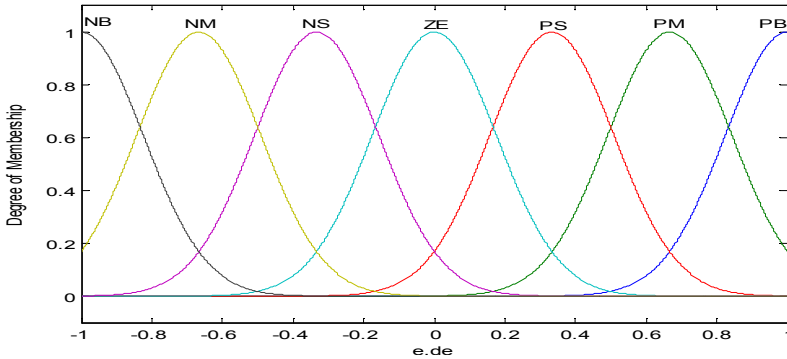


Fig. 6. Membership functions for inputs “e” and “de”.

where: d : Desired torque controller G_{em}^* (Output of SMC controller) and y : Actual output (y is equal to output of NFLC (G_{em-NFC})).

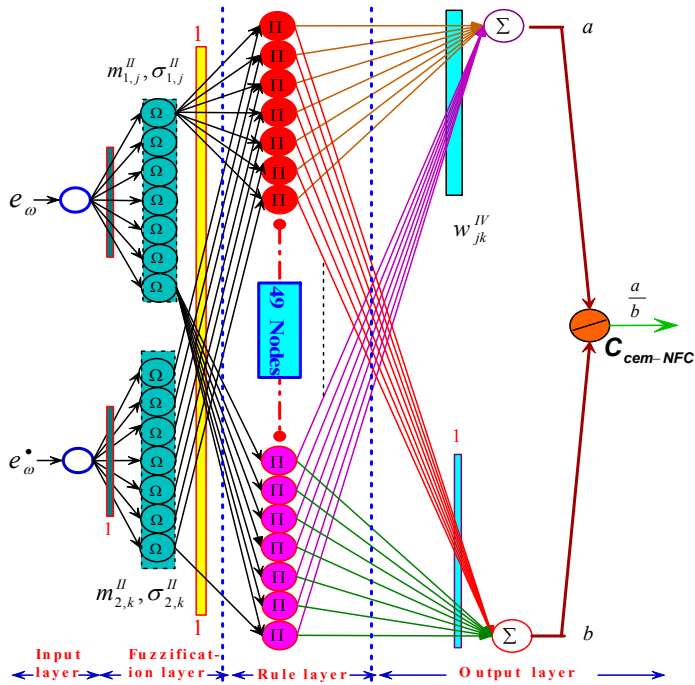


Fig. 7. NFC network building.

6. Simulation results

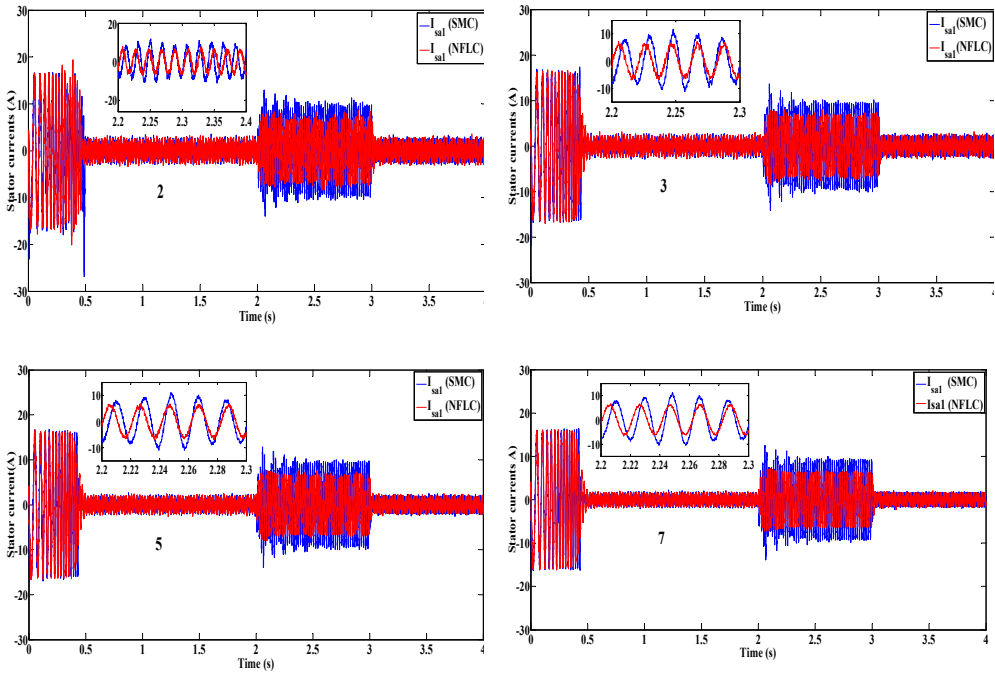


Fig.8. Simulated responses of outputs current for different number of levels m , with increased rotor resistance ($\Delta Rr^0 = +50\%$) followed by applying load torque (14N.m).

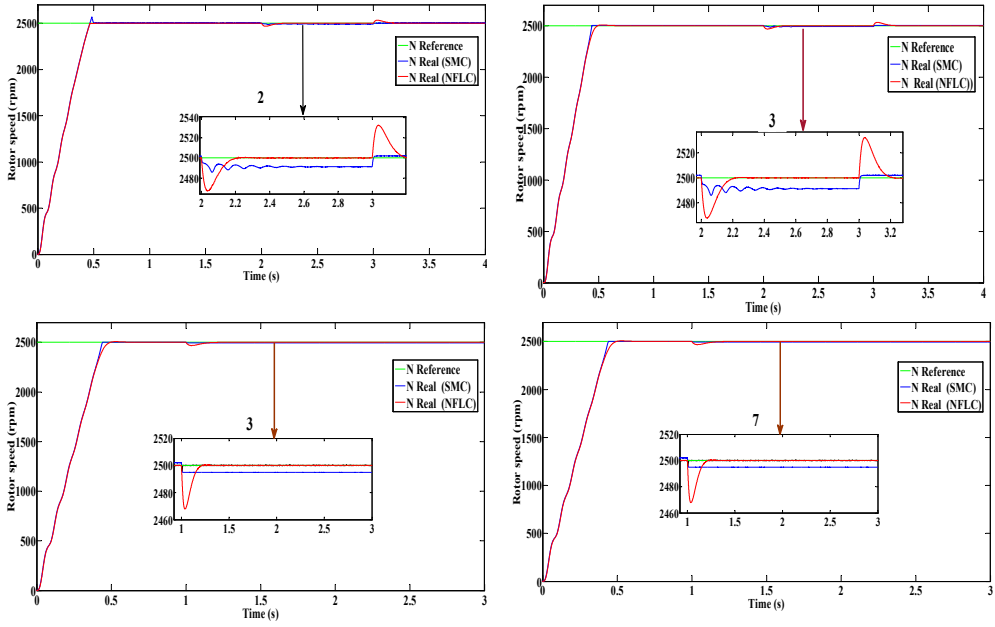


Fig. 9. Simulated responses of the rotor speed for different number of levels m with increased rotor resistance ($\Delta R_r\% = +50\%$) followed by applying load torque (14N.m).

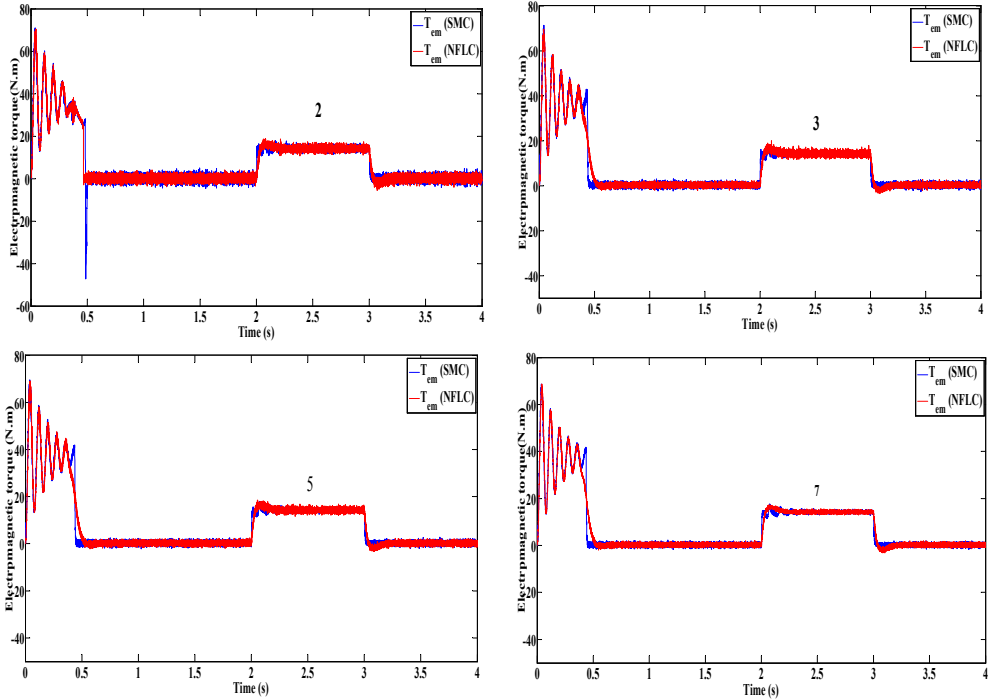


Fig. 10. Simulated responses of the electromagnetic torque for different number of levels m , with increased rotor resistance ($\Delta R_r\% = +50\%$) followed by applying load torque (14N.m).

Fig. 8 presents the stator current per phase for converters with varying levels from $m = 2$ to $m = 7$. At $t = 2s$, a load of $Cr = 15N.m$ is applied. To assess robustness, we conducted tests using the SMC and NFLC controller, with the rotor resistance (R_r) undergoing a variation of $R_n + 50\%$ after $t = 2s$. The findings reveal a noteworthy trend: as the number of levels decreases, the output voltage progressively approaches a more ideal sinusoidal waveform. This suggests that reducing the number of levels in the converter has a positive impact on achieving a better sinusoidal output.

Fig. 9 compares the performance of the proposed NFLC with the SMC approaches for the DSIM. The figure demonstrates the remarkable robustness of all three controllers in maintaining speed regulation even under significant disturbances. These disturbances include a 50% increase in rotor resistance ($\Delta R_r = +50\%$) at 2 seconds and the application of a 15 Nm load torque ($Cr = 15 Nm$) at the same time. Notably, the speed response of the DSIM with all three controllers remains unaffected by these changes.

The results presented in Fig. 10 reveal a continuous and gradual decrease in electromagnetic torque ripple in steady state as the number of levels in the converters increases, coupled with variations in the rotor resistance. Notably, as the inverter voltage level rises from $m=2$ to $m=7$, the electromagnetic torque ripple experiences a significant reduction. This suggests a positive correlation between the number of levels in the converters and the mitigation of electromagnetic torque ripple. Together simulation results indicate that the proposed NFLC controller gives better performances and robustness than the SMC controllers. It is observed a substantial reduction in the magnitude of pulsations in the electromagnetic torque and stator currents with a multi-level inverter compared to a conventional inverter.

The simulation results convincingly demonstrate a key strength of the NFLC: its remarkable insensitivity to constant variations in resistance. This stands in stark contrast to SMC controllers, which exhibit differing responses under similar conditions. This superior robustness suggests that the NFLC may be a more effective control strategy across a wider range of operating scenarios. This includes situations traditionally managed by SMC methods, potentially offering improved performance and stability in these applications.

7. Experimental validation

The experimental validation was conducted using a double-star induction machine at the Electrical Drives Systems Laboratory (LSEE) of the Polytechnic School (EMP). The machine is obtained by rewinding a conventional three-phase asynchronous machine. The electrical and mechanical parameters match those in the simulation (Table 2, Annex 1). See Fig. 11 for the experimental test bench photo. So, the double-star induction machine is powered by two three-phase two-level voltage inverters. The DC bus voltage is derived from rectifying the three-phase mains voltages. Sinusoidal triangular pulse width modulation (MLI) is employed to generate control commands for the power electronics switches at a 10 kHz switching frequency. Control is executed through a dSPACE 1104 real-time control board utilizing the Control Desk real-time control environment. The machine speed is monitored by a tachometer generator, and sensor cards along with signal conditioning for currents and voltages facilitate the acquisition and conditioning of these parameters.

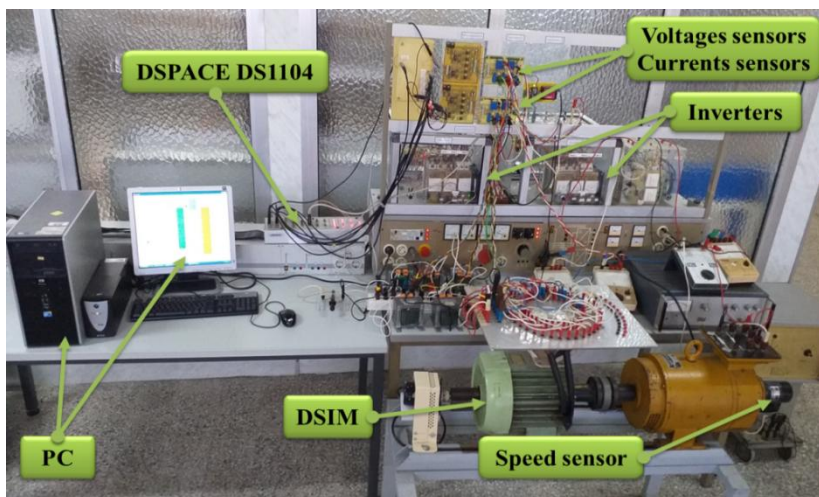


Fig. 11. Experimental test bench.

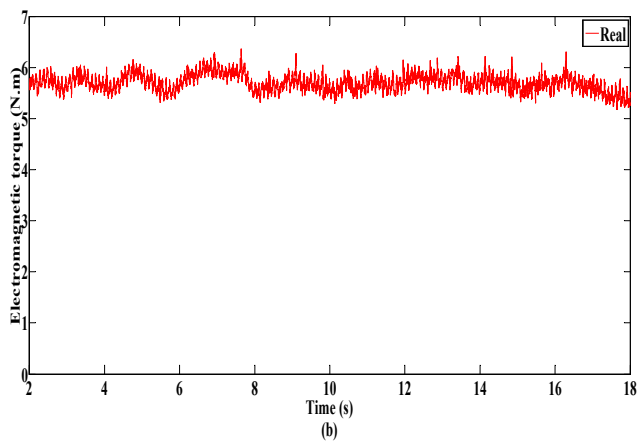
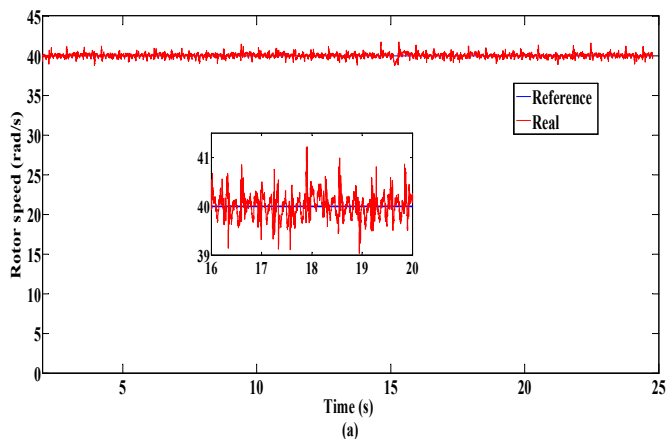


Fig. 12. Zoomed of experimental responses of rotor speed and electromagnetic torque for two levels inverters, with increased rotor resistance ($\Delta R_r\% = +50\%$) followed by applying load torque (6N.m), with SMC controller.

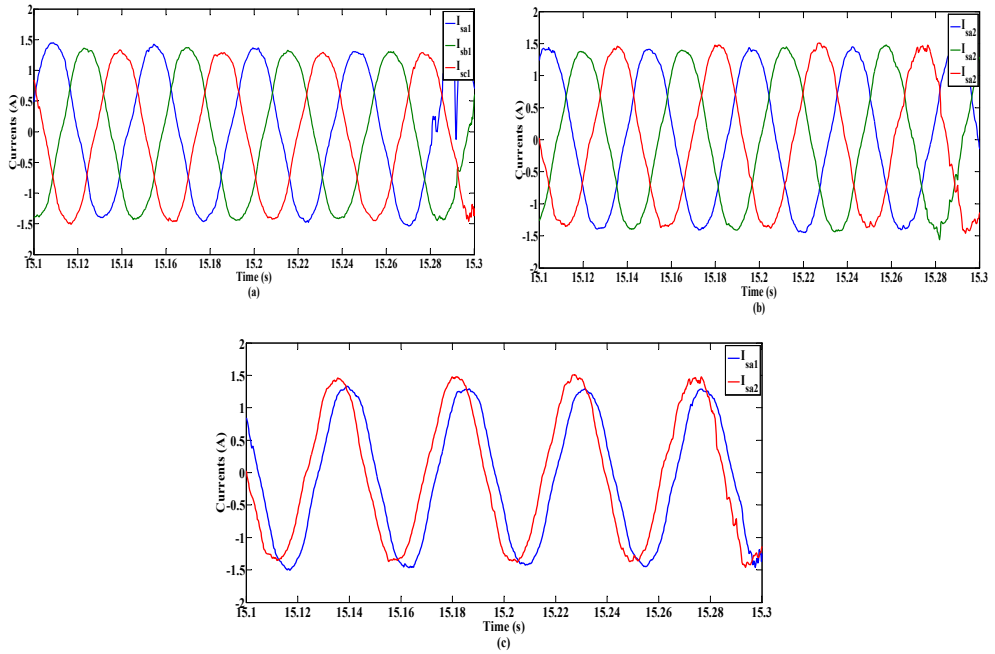


Fig.13. Zoomed of experimental responses of outputs currents for two levels inverters, with increased rotor resistance ($\Delta R_r\% = +50\%$) followed by applying load torque (6N.m), with SMC controller

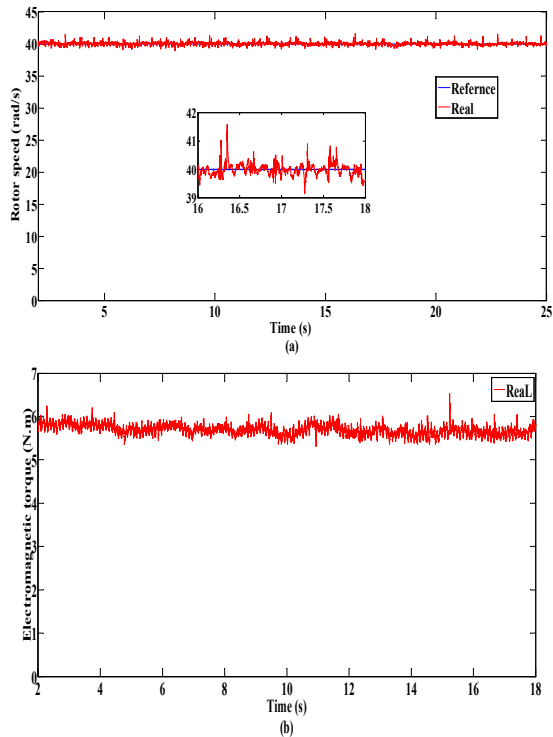


Fig.13. Zoomed of experimental responses of rotor speed and electromagnetic torque for two levels inverters, with increased rotor resistance ($\Delta R_r\% = +50\%$) followed by applying load torque (6N.m), with NFLC controller.

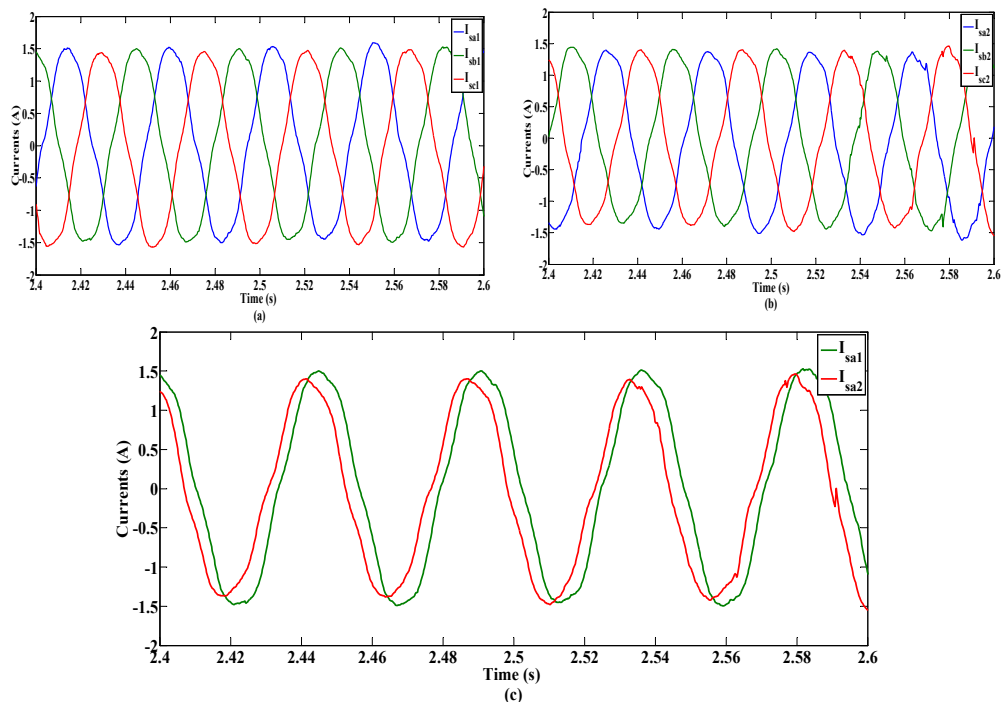


Fig.14. Zoomed of experimental responses of outputs currents for two levels inverters, with increased rotor resistance ($\Delta R_r\% = +50\%$) followed by applying load torque (6N.m), with NFLC controller.

Testing both Neuro-Fuzzy logic control and sliding mode control on a DSIM driving a water pump yielded satisfactory steady-state performance. Both controllers maintained the desired speed with minimal error. However, NFLC exhibited slightly superior steady-state accuracy, particularly under fluctuating loads. Notably, NFLC significantly outperformed SMC in terms of dynamic response. It demonstrated faster reaction times, quicker stabilization periods, and reduced overshoot during transient events. This superior dynamic performance stems from NFLC ability to adapt to changing system behavior and handle uncertainties. However, designing an effective NFLC requires expertise in selecting appropriate fuzzy membership functions and neural network parameters, which can be an iterative process.

8. Conclusion

The present paper presents an innovative design that utilizes the NFLC for regulating the speed and phase currents of the DSIM driving a water pump fed by MLC. The NFLC control offers several advantages, including high performance, simplicity in composition, robustness against disturbances, and improved tracking performance of speed and phase currents compared to the SMC controller. The results obtained by different levels of MLC providing output voltages at a predefined level improve the shape of the voltages feeding the DSIM. The control of the fuzzy system, implemented with four-layer NN architecture and using the speed error and its derivative as inputs, was successfully employed. The learning process of the NFLC relied on the gradient descent technique. The simulation and

experimental results unequivocally demonstrate the superiority of the NFLC over the SMC controller in terms of robustness. Furthermore, the proposed controller exhibited high reliability and efficiency in regulating the speed of the DSIM under various operating conditions and increasing levels.

APPENDIX 1

Table. 2: Dual star induction machine parameters for simulation.

Quantity	Symbol and magnitude
Rated power Pn	4.5 kW
Rated voltage Vn	220/380 V
Rated current In	6 A
Rated speed Nn	2753 rpm
Number of poles P	2
Rated frequency f	50 Hz
Stator resistance Rs	3.72 Ω
Rotor resistance Rr	2.12 Ω
Stator inductance Ls	0.022 H
Rotor inductance Lr	0.006 H
Mutual inductance Lm	0.3672 H
Moment of inertia J	0.0662 kg.m2
Coefficient of viscous friction f	0.006 N.m.s/rad

REFERENCES

[1] E. Zaidi, A. Reffas, H. Talhaoui, O. Aissa, R. Zouache, K. Marouani and M. Becherif, “New PI- synergetic hybrid control for suppressing circulating currents of an electrical drive system fed by two parallel inverters”, *Electrical Engineering*, vol. 106, no. 3, 2024.DOI: [10.1007/s00202-024-02617-z](https://doi.org/10.1007/s00202-024-02617-z)

[2] E. Zaidi, K. Marouani, H. Bouadi1, K. Nounou, and M. Becherif,“ Circulating current reduction based hybrid controller of an electrical drive system fed by two parallel inverters”, *Electrical Engineering*, vol. 103, no. 1, pp. 205-216, 2021.DOI : [10.1007/s00202-021-01284-8](https://doi.org/10.1007/s00202-021-01284-8)

[3] E. Zaidi, K. Marouani, H. Bouadi, L. Bentouhami, and E. Merabet, “Fuzzy Sliding Mode Method for Speed regulation of a Dual Star Induction Machine Drive fed by Multi-level Inverters”, In *IEEE 2018 International Conference on Applied Smart Systems (ICASS2018)*, 2018.DOI: [10.1109/ICASS.2018.8651948](https://doi.org/10.1109/ICASS.2018.8651948)

[4] E. Zaidi, K. Marouani, H. Bouadi, K. Nounou, M. Aissani, and L. Bentouhami, “Control of a Multiphase Machine Fed by Multilevel Inverter Based on Sliding Mode Controller”, In *IEEE-EEEIC: 19thInternational Conference on Environment and Electrical Engineering (EEEIC2019)*, 11-14 June 2019, Genoa, Italy, 2019.DOI: [10.1109/EEEIC.2019.8783559](https://doi.org/10.1109/EEEIC.2019.8783559)

[5] E. Zaidi, K. Marouani, and H. Bouadi, “Speed Control for Multi-phase Induction Machine Fed by Multi-level Converters Using New Neuro-Fuzzy”, *Chapter books, Springer Nature Switzerland AG* 2019, ICAIRES 2018, vol. 62, pp. 457-468, 2019.doi.org/10.1007/978-3-030-04789-4_49

[6] G.Feng, C. Lai,M. Kelly and N.C.Kar, “Dual three-phase PMSM torque modeling and maximum torque per peak current control through optimized harmonic current injection”, *IEEE Trans. Ind. Electron.* vol. 66, no. 5, pp. 3356-3368, 2018. DOI: [10.1109/TIE.2018.2854550](https://doi.org/10.1109/TIE.2018.2854550)

[7] M. A.Frikha, J.Croonen, K. Deepak, Y.Benômar, M. El Baghdadi and O. Hegazy, “Multiphase motors and drive systems for electric vehicle powertrains: State of the art analysis and future trends”, *Energies*, vol. 16, no. 2, 768, 2023.doi.org/10.3390/en16020768

[8] R. Belal, M. Flitti, and M. L. Zegai, “Tuning of pi speed controller in direct torque control of dual star induction motor based on genetic algorithms and neuro-fuzzy schemes”,*Revue Roumaine des Sciences Techniques SérieÉlectrotechnique et Énergétique*, vol. 69, no. 1, pp. 9-14, 2024.doi.org/10.5927/RRST-EE.2024.1.2

- [9] B. Lyas, O. Bouhali, S. Khadar and Y. Mohammed, "A novel dual three-phase multilevel space vector modulation for six-phase multilevel inverters to drive induction machine", *Modelling, Measurement and Control*, vol. 92, no. 2-4, pp. 79-89, 2019.doi.org/10.18280/mmc_a.922-407
- [10] F.Z. Khemili, M. Lefouili, O. Bouhali, N. Rizoug and L. Bekrar, "Dual three phase multilevel space vector modulation control of diode clamped inverter for dual star induction motor drive", *Journal Européen des Systèmes Automatisés*, vol. 55, no. 5, pp. 603-613, 2022.[DOI : 10.18280/jesa.550505](https://doi.org/10.18280/jesa.550505)
- [11] G. Boukhalfa, S. Belkacem, A. Chikhi, and S. Benagoune, "Genetic algorithm and particle swarm optimization tuned fuzzy PID controller on direct torque control of dual star induction motor", *Journal of Central South University*, vol. 26, no. 7, pp. 1886-1896, 2019.doi.org/10.1007/s11771-019-4142-3
- [12] E. Zaidi, K. Marouani, H. Bouadi, L. Bentouhami, and E. Merabet, "Fuzzy Sliding Mode Method for Speed regulation of a Dual Star Induction Machine Drive fed by Multi-level Inverters", *In IEEE 2018 International Conference on Applied Smart Systems (ICASS2018)*, 24-25 November 2018, Médéa, Algiers, Algeria, 2018.[DOI: 10.1109/ICASS.2018.8651948](https://doi.org/10.1109/ICASS.2018.8651948)
- [13] U. Michael, T. Wishart, and R. G. Harley, "Identification and Control of Induction Machines Using Artificial Neural Networks", *In: IEEE Transactions on Industry Applications*, vol. 31, no. 3, pp. 612 - 619, 1995.[DOI: 10.1109/28.382123](https://doi.org/10.1109/28.382123)
- [14] M. Bouziane, M. Abdelkader, "Direct space vector modulation for matrix converter fed dual star induction machine and Neuro-fuzzy speed controller", *Bulletin of Electrical Engineering and Informatics*, vol. 8, no.3, pp. 818-828, 2019.doi.org/10.11591/eei.v8i3.1560
- [15] M. N. Uddin, M. A. Abido, and M. A. Rahman, "Development and implementation of a hybrid intelligent controller for interior permanent magnet synchronous motor drive", *Transactions on Industry Applications*, vol. 40, no. 1, pp. 68-76, 2004.[DOI: 10.1109/IAS.2002.1042745](https://doi.org/10.1109/IAS.2002.1042745)
- [16] E. Zaidi, K. Marouani, H. Bouadi, K. Nounou, M. Aissani, and L. Bentouhami, "Control of a Multiphase Machine Fed by Multilevel Inverter Based on Sliding Mode Controller", *In IEEE-EEEIC: 19th International Conference on Environment and Electrical Engineering (EEEIC2019)*, 11-14 June 2019, Genoa, Italy, 2019.doi.org/10.11591/eei.v8i3.1560
- [17] E. Zaidi, K. Marouani, A. E Mabrek, E. Merabet and L. Bentouhami, "Fuzzy Logic Control of Multi-Phase Induction Machine Drives Based on Cascaded Hybrid Multi-level Inverters," *In IEEE the International Conference on Electrical Sciences and Technologies in Maghreb CISTEM 2018*, USTHB-Algiers, Algeria, 29-31 October 2018.[DOI: 10.1109/CISTEM.2018.8613481](https://doi.org/10.1109/CISTEM.2018.8613481)
- [18] E. Zaidi, K. Marouani, and H. Bouadi, "Simulation and Analysis of DSI Speed Control System Supplied by Multi-Level Converter Using Fuzzy Logic Controller", *In IEEE 2019 International conference on Advanced Electrical Engineering November (ICAEE'19)*, 19-21 November 2019, El Hamma, Algiers. Algeria, 2019.[DOI: 10.1109/ICAEE47123.2019.9015153](https://doi.org/10.1109/ICAEE47123.2019.9015153)